Seismic evidence of bending and unbending of subducting oceanic crust and the presence of mantle megathrust in the 2004 Great Sumatra earthquake rupture zone

Satish C. Singh[1], Ajay P. S. Chauhan[1], Andrew J. Calvert[2], Nugroho Hananto[1], Dibakar Ghosal[1], Abhishek Rai[1], Helene Carton[3]

1. Laboratoire de Géosciences Marines, Institut de Physique du Globe de Paris, Sorbonne Paris Cité, Paris 75236, France

2. Department of Earth Sciences, Simon Fraser University, Burnaby, BC V5A 1S5, Canada

3. Lamont Doherty Earth Observatory, Columbia University, Palisades NY 10964-8000, USA

Corresponding author: singh@ipgp.fr, Tel: +33 1 83957658

In subduction zones the plate interface (megathrust) is typically poorly imaged at depths > 12 km, however its precise geometry and nature as well as the positions of updip and downdip limits of the seismogenic zone are important elements to understand the generation of megathrust earthquakes. Using deep marine seismic reflection and refraction data, we observed discontinuous reflections off the top of the subducting oceanic crust down to 60 km depth in the 2004 great Sumatra-Andaman earthquake rupture zone. We find that the top of the downgoing plate does not dip gently into the subduction zone but instead displays a staircase

geometry with three successive, 5-15 km vertical steps, spaced ~50 km apart. Micro-earthquake data indicate that most of the seismicity lies below this interface, suggesting that the oceanic plate is deforming actively. Along part of the profile, we also image a second reflector located 8-10 km below the top of the oceanic crust. The forward modelling of the gravity data along the profile supports the presence of a high-density material above this reflector. The presence of a staircase shape for the top of the oceanic crust, together with constraints from gravity data and earthquake data, require that the megathrust goes through this second reflector. This leads us to conclude that the megathrust is at least partly located in the oceanic mantle and that underplating of oceanic crust beneath the wedge and underplating of upper mantle beneath the forearc basin are taking place in this region.

Key words: megathrust, subduction zone, Sumatra earthquake, seismogenic zone, underplating, thrust faulting

1. Introduction

The 26th December 2004 Mw=9.3 earthquake was one of the largest earthquakes in the last forty years. It initiated offshore Simeulue Island, SW of the tip of Sumatra, and ruptured over 1300 km of the plate boundary from northern Sumatra to the Andaman Islands (Ammon et al, 2005). The earthquake generated a devastating tsunami that took more than 230,000 lives and caused havoc around the Indian Ocean. Co-seismic slip modelling studies suggest that the maximum slip occurred north of the epicentre either

47 just south of the Aceh forearc basin (Chlieh et al., 2007) or near the subduction front
48 (Rhie et al., 2007) (Figure 1). Aftershock data recorded using teleseismic network show
49 two intriguing patterns: (1) steeply dipping thrust events all along the deformation front
50 and (2) a cluster of steeply dipping thrust events beneath the Aceh basin (Figure 1)
51 (Engdahl et al., 2007; Pesicek et al., 2010). Based on a deep seismic reflection profile
52 acquired near the epicentral area, Singh et al. (2008) suggested that the 2004 megathrust
53 earthquake (pure thrust event with a dip of ~12°) ruptured a mantle megathrust that cuts
54 through the oceanic crust at steep angles near and seaward of the deformation front.
55 However, the presence of steeply dipping thrust events beneath the Aceh basin remains
56 an enigma.
57
58 Near the epicentre of the great Sumatra-Andaman earthquake, the Indo-Australian
59 oceanic plate subducts obliquely beneath the Sunda continental plate at a rate of 53
60 mm/yr, decreasing to 43 mm/yr at the latitude of the Andaman Islands (Prawirodirdjo et
61 al., 2000). The obliquity of the convergence, which increases northward from 20° near
62 the epicentre to nearly parallel plate motion west of the Andaman Islands, leads to a slip
63 partitioning between pure thrust orthogonal to the trench and strike-slip displacement
64 parallel to the subduction front (Fitch, 1972). The seismic activity and the linear shape of
65 the great Sumatra fault (GSF) seem to accommodate significant part of the dextral motion
66 (McCaffrey et al., 2000; Sieh et al., 2000), and possibly along the West Andaman Fault
67 (WAF) (Singh et al., 2005; Chauhan et al., 2009) and Mentawai Fault (Diament et al.,
68 1992). Further northwards, the GSF joins the WAF that is linked with the Sagaing fault
69 (Kamash Raju et al., 2004) through a series of spreading centres and transform faults in

70 the Andaman Sea. The present day subduction in the Sumatra region has been in place at
71 least since middle tertiary time (~30 My) (Hamilton, 1988), with the subduction history
72 extending back to late Palaeozoic (Katili, 1973). Thick sediments from the Bengal fan
73 have led to the development of a very wide accretionary wedge in the northern Sumatra-
74 Andaman region (Singh et al., 2008; Franke et al., 2008).
75
76 At ~150 km south of the 2004 earthquake epicentre, an earthquake of Mw=8.5 had
77 occurred in 1861 and the same patch ruptured again in 2005 (Mw=8.7) (Briggs et al.,
78 2006). Further south, offshore central and southern Sumatra, two large earthquakes
79 (1797, Mw=8.4; 1833, Mw~9.0) have been reported, and more recently in 2007
80 (Mw=8.5) (Konka et al., 2008). Based on coral data, Sieh et al. (2008) suggested that the
81 western Sumatra subduction zone is segmented and great earthquakes could occur every
82 200-250 years along each segment. However, no great earthquakes were reported in the
83 2004 earthquake rupture zone, and hence it was surprise when the 2004 earthquake
84 ruptured the whole section from northern Sumatra all the way to Andaman Islands.
85
86 In the aftermath of the 2004 earthquake and tsunami, a series of marine surveys were
87 carried out by different international groups (Araki et al., 2006; Henstock et al, 2006;
88 Sibuet et al., 2007; Franke et al., 2007; Graindorge et al., 2009), which provided
89 bathymetry and seismic images down to 10 km depth. In order to image the deep
90 structures down to 60 km depth, we carried out a joint deep seismic reflection and
91 refraction survey in the maximum slip region of the 2004 earthquake. A deep seismic
92 profile (WG1) in vicinity of the 2004 earthquake epicentre showed that the subudcting

93 oceanic plate breaks as it subducts, which led Singh et al. (2008) to suggest that the 2004
94 megathrust rupture might be in oceanic mantle, not at the oceanic igneous crust and
95 accretionary sediment interface. Using seismic refraction data along the same profile
96 Dessa et al. (2009) found that the continental crust there is thin (20-25 km), suggesting
97 that the 2004 earthquake rupture should have either initiated in the mantle wedge or in
98 the oceanic mantle underneath. Here, we present crustal and upper mantle structure
99 results obtained along profile WG2, which crosses the subduction system from the
100 subduction front to the Great Sumatra Fault and volcanic arc in the Andaman Sea (Figure
101 1). We interpret these structures using additional constraints from relocated aftershocks
102 and gravity data.
103
104 **2. Seismic reflection data and results**
105
106 Deep seismic reflection data were acquired by the seismic vessel *Geco Searcher* of
107 WesternGeco (a seismic company) in July 2006. An airgun array consisting of six sub-
108 arrays containing a total of 48 airguns with a total volume of 10,700 in^3 was deployed at
109 15 m water depth. A Q-Marine streamer, 12 km long, was deployed at 15 m depth. A Q-
110 Marine• streamer, a new generation of single sensor technology of Schlumberger, is
111 equipped with hydrophones spaced every 3.125 m. The data were digitized and low-cut
112 filtered (2 Hz) in-sea prior to being transmitted to the on-board recording system. After
113 applying proprietary digital noise attenuation techniques and an appropriate digital spatial
114 anti-alias filter, the digital signals were spatially resampled to a 12.5-m receiver interval,

115 thus providing 958 channels. The data were recorded with a sampling interval of 2 ms
116 and a trace length of 20.48 s. The vessel speed varied from 4.2 to 4.8 knots.
117
118 The data were processed using a specialised processing strategy aimed at emphasising the
119 low frequencies to optimise deep crustal imaging (Singh et al., 2008). The data were
120 resampled to 8 ms. Swell noise was removed while preserving low frequencies above 2.5
121 Hz. Six passes of cascaded Radon multiple removal technique (Foster and Mosher, 1992)
122 were applied to remove the water bottom multiples. A combination of constant velocity
123 analysis and semblance velocity analysis were performed at 1 km intervals after each
124 pass of Radon multiple removal to determine the stacking velocities. The data were
125 stacked and migrated using a post-stack Kirchhoff migration technique.
126
127 Figure 2 shows the seafloor bathymetry, non-interpreted and interpreted seismic images
128 along profile WG2. The profile is 445 km long and is approximately 20° from being
129 orthogonal to the trench. The seafloor at the trench is nearly flat at a water depth of 4.55
130 km whereas the frontal section of the accretionary prism is very steep and the water depth
131 decreases to 337.5 m at the frontal ridge within 45 km from the trench. The northeast side
132 of the frontal ridge is very steep, and the water depth increases to 1600 m. The
133 accretionary wedge is ~125 km wide, and looks like a plateau with an average water
134 depth of 1400 m, bounded by the frontal ridge in the southwest and the forearc high in the
135 northeast, the shallowest point of which lies at 360 m water depth. Within the plateau,
136 one can identify two gently seaward-dipping large-scale (~55 km) bathymetric features
137 with slightly different slopes (S1 and S2); the second one (S2) defines the southwest

138 margin of the forearc high. The northeast margin of the forearc high is steep and bounds
139 the Aceh forearc basin, which lies at 2700 m water depth and is ~22 km wide. The
140 Sumatra Platform represents the offshore extension of the Sumatra continental block,
141 gently sloping southwestward, where the water depth varies from 1800 m in SW to 1500
142 m in NE. The offshore extension of the Sumatra Fault is defined by ~18 km wide flat
143 basin at 1900 m water depth whereas the volcanic arc lies in a 3400 m deep 22 km wide
144 basin with volcanoes in its centre. Further northeast, the bathymetry smoothly decreases
145 to 1500 m at the end of the profile in the Andaman Sea.
146
147 On the oceanic plate, the sediment thickness increases from 2 s two-way travel time
148 (TWTT) to 3.2 s near the deformation front. The reflector at ~8.2 s (Figures 2, 3a) is the
149 top of the oceanic crust. Weak reflection at 1.5 s below the basement is the oceanic
150 Moho (Singh et al., 2011a). The deformation front is located at the base of the frontal
151 slope where the largely intact incoming stratigraphy begins to deform as it is incorporated
152 into the accretionary prism. Although the upper 3 s of the frontal ridge consists of steeply
153 landward dipping sediments, the basin just NE of the ridge contains ~3 s of nearly sub-
154 horizontal sediments (Figure 3a) that have a character similar to the sediments near the
155 deformation front. With the exception of the uppermost sedimentary section, which
156 reveals folding and faulting within 0.5 s of the seafloor, the rest of the accretionary
157 plateau is non-reflective. A package of seaward dipping reflections beneath the forearc
158 high is interpreted to be from backthrusts (Chauhan et al., 2009) and the deepest of these
159 reflections is the continental backstop (Figure 3b). The sediments in the forearc Aceh

basin are ~ 1 s thick and the basement gently dips seaward, and seems to be continuous with the backstop.

The top of the igneous oceanic crust is weakly imaged beneath the frontal slope, but a landward dipping reflection is observed within the oceanic crust at 9.5-10.5 s at the deformation front (Figure 3a); this reflection may indicate the faulting of oceanic crust that has been interpreted further south (Singh et al., 2008). The top of the igneous oceanic crust is identified beneath the accretionary wedge along most of the profile, and it can be traced landward to a depth of 12 s beneath the forearc high (Figure 2, 3b). Beneath the Aceh forearc basin, two reflections can be identified at 11.5 s and 13 s; we interpret the upper reflection to be from the continental Moho and the deeper reflection to be from the top of the subducted oceanic plate. The upper reflection continues northeastward beneath the Sumatra Platform, but the lower reflector is discontinuous. Further northeast, a strong sub-horizontal reflection is imaged at ~18 s beneath the Sumatra Platform (Figure 2). The strike-slip Sumatra Fault is marked with flower structures (Ghosal et al., 2009). In the Mergui backarc basin, a sedimentary section up to 3 s thick is present. The continental Moho can be identified at 10 s beneath the Mergui Basin. Just northeast of the volcanic arc, some 3-5 km long sub-horizontal reflections are present between 13 and 15 s, and we suggest that these represent melt lenses in the uppermost mantle.

3. Seismic refraction results

182 The seismic refraction data along profile WG2 was acquired by the R/V Marion Dufrense
183 in 2006. Fifty-six ocean bottom seismometers (OBS) were deployed at an interval of 8.1
184 km along the profile. An array of 18 airguns with a total volume of 8100 cubic inch tuned
185 in single bubble mode (Avedik et al., 1993) was used as an energy source. The shot
186 interval was 150 m. An example of data recorded by an OBS placed on the forearc high is
187 shown in Figure 4. These data clearly show the low velocity from accretionary wedge
188 sediments, and reflections from the top of the oceanic crust and continental Moho.
189
190 First arrivals were picked and inverted using an adaptive travel time tomography
191 technique, where the model is parameterised using a triangular grid (Trinks et al, 2005).
192 A total of ~30000 picks were used. The picking uncertainty was in the range of 50-180
193 ms. A 1D velocity model with a linear velocity gradient was used as a starting model.
194 Initially, a large triangle size (5 km) was used, which was then reduced to 1.25 km. A
195 smoothing regularisation was applied, which varied with the triangle size. The initial
196 smoothing was kept large, 50 km horizontal and 5 km vertical using a 2D Gaussian
197 function, which was reduced to 15 km horizontally and 2 km vertically during the final
198 inversion stage. Wide-angle reflection data were then included in the inversion to
199 constrain the top of the downgoing plate, oceanic and continental Moho. The initial travel
200 time misfit was between -2500 ms and +3000 ms, which was reduced to a root mean
201 square misfit value of 132 ms after 10 iterations (Figure 5), similar to the misfit (156 ms)
202 achieved by Dessa et al. (2009) along a profile 240 km further south. These data allow us
203 to determine P-wave velocities down to 20 km depth beneath the oceanic crust and 30 km
204 beneath the accretionary wedge and continental crust (Figure 6a). A significant part of

205 model was well constrained by 250-350 rays except in a narrow zone below 15 km depth
206 at 350 distance range due to the absence of data at two OBS (Figure 6b). We have used
207 the diagonal elements of the inverse of the Hessian matrix to estimate the uncertainly in
208 the final model (Hobro et al., 2003), which indicates that that uncertainty in the resulting
209 model lies between 400 m/s and 800 m/s (Figure 6c). As noted by Hobro et al. (2003),
210 this approach generally over estimates the uncertainty in the model, and therefore, we
211 suggest that the region with uncertainly less than 800 m/s is well contained by the
212 inversion. It should be noted that sharp changes in velocity, which often occur at the top
213 of the igneous crust, tend to be smoothed out in tomographic velocity models. The details
214 of the tomographic method can be found in Chauhan (2010) and will be published
215 elsewhere.
216
217 Inverted P-wave velocities in the uppermost sedimentary sections, where seismic
218 reflections are often observed, are 1.6-3.5 km/s (Figure 6). Within the accretionary
219 wedge, the 4 km/s iso-velocity contour is ~3 km below the seafloor, consistent with the
220 presence of dewatered sediments that extend to the top of the underlying igneous crust
221 where sediment velocities attain their maximum values of 5.0-5.5 km/s, implying a
222 wedge thickness of ~13 km. Wide-angle reflections from the top of the igneous oceanic
223 crust coincide with the 6 km/s velocity contour down to 16 km depth (Figure 6). The
224 wide-angle reflection from the oceanic Moho is observed below the deformation front,
225 and locates the Moho about 5 km below the basement, consistent with thin crust reported
226 by Singh et al. (2011a). The most striking feature of the derived velocity model is the
227 landward shallowing of the 5.5 km/s iso-velocity contour by 8 km beneath the forearc

basin. This seaward dipping contour correlates closely with the deepest inferred backthrust and indicates a sudden lateral change in lithology consistent with the existence of the continental backstop, as suggested by Chauhan et al. (2009). With the exception of changes in thickness of the sedimentary layer, the crust to the northeast exhibits little lateral velocity variation, and velocity values are consistent with the presence of thinned continental crust. In the backarc region, wide-angle reflections interpreted to be from the continental Moho originate at a depth of ~18 km and coincide with the 7 km/s velocity contour.

4. Depth Converted Reflection Image

The well-constrained velocity model for the upper 30 km was extended to 70 km using a mantle velocity of 8 km/s, which was used to depth convert the seismic reflection data, allowing the dip of the downgoing plate to be estimated (Figure 7). In the ocean basin, the reflection from the top of the igneous oceanic crust (basement) corresponds to a P-wave velocity of ~4.5 km/s; however, there are only weak reflection from the oceanic Moho ~5 km below the basement (Singh et al., 2011a), consistent with the wide-angle inversion results (Figure 6). The dip of the downgoing plate is 2° seaward of the deformation front. It is interesting to note that the two well imaged parts of the top of the oceanic crust beneath the accretionary wedge (F1) and forearc high (F2) are nearly sub-horizontal and seem to be offset by >5 km. The reflector F1 coincides with the top of the oceanic crust determined from wide-angle data. Their dip is ~3-5°, in contrast to the inferred dip of 12° of the 2004 earthquake rupture. These two reflectors are collocated

with the seaward dipping bathymetric slope observed in the accretionary plateau (S1 and S2 in Figure 2a). The dip of the backthrust is ~30-40° in the upper 15 km and it decreases to 15° above the F2 reflector. We do not observe any strong landward dipping reflector beneath the accretionary plateau that could be interpreted as an out of sequence fault (splay fault) as suggested by Sibuet et al. (2007).

The seismic velocity between the backthrust and F2 reflector is >6.0 km/s, which suggests that this block could be the seaward continuation of the continental crust or, alternatively, a block of oceanic crust underplated to the forearc (Calvert et al., 2006; Singh et al., 2008). Sub-horizontal reflections beneath the Aceh basin, which are interpreted to be from the continental Moho, lie at ~25 km depth and coincide with the 7.8 km/s velocity contour, suggesting that the overriding crust is 23 km thick here, which is consistent with the crustal thickness observed further south (Dessa et al., 2009). The reflector underneath the continental Moho at 33-38 km is also shallow dipping (F3) (10°). Interestingly, a 50 km long shallow dipping reflection (~8.5°) is imaged at 55-58 km depth (F4). There are two reflectors at 20-22 km depth beneath the accretionary prism, which might be the oceanic Moho or mantle megathrust (Singh et al., 2008).

Beneath the Sumatra Platform, there are two sub-horizontal reflectors at ~25 km depth, which may correspond to the continental Moho. At the northeastern end of the profile, a reflection is present at 22 km depth, a couple of kilometres below the continental Moho determined from wide-angle reflection data (Chauhan, 2010). This discrepancy between reflection and wide-angle crustal thickness could be due to small error in crustal velocity.

5. Teleseismic events and micro-earthquakes

Aftershocks of a large earthquake could either occur in the ruptured zone or at the extremity of the main rupture, but the accurately located aftershocks of the 2004 megathrust earthquake around profile WG2 lie in a broad zone covering the maximum slip during the main rupture (Pesicek et al., 2010), suggesting that they represent active deformation in the ruptured zone. Similarly, a significant number of teleseismic events before the 2004 earthquake coincide with the maximum slip. Therefore, we use the seismicity before and after the 2004 earthquake to provide some insight about active deformation in the light of the new deep seismic image. Here we show relocated micro-seismic data from the 2005 OBS deployments and teleseismically located events between 1997 and 2005 (Engdahl et al., 2007; Pesicek et al., 2010).

Twenty short-period OBS were deployed offshore northern Sumatra during the Sumatra Aftershock experiment from15 July to 9 August 2005. The OBS array covers a zone of about 370 km x 75 km across the Sumatra subduction system from the subduction front to the volcanic arc. Data was recorded continuously during the whole duration of the experiment. More than 1000 events were extracted manually from the continuous record of each OBS. Micro-earthquake recorded on four or more seismic stations were selected for further processing. The 2D velocity model along line WG2 (Figure 6) was used to create a three-dimensional velocity model for the region. It was assumed that the 2D velocity structure does not change significantly in a 100 km wide zone on either side of

297 profile WG2. The extrapolated 2D velocity profiles were centred at the subduction front
298 so that the offsets from the subduction front remains constant while preparing the 3D
299 velocity model. We relocated the events in the 3D velocity model using an iterative,
300 damped least-square algorithm (Thurber and Eberhart Phillips, 1999). We used at least
301 four P- and one S-wave arrivals to locate the micro-earthquakes. Magnitudes of the
302 micro-earthquakes were computed from the duration of seismic waves (Araki et al,
303 2007), which varied from -1 to 7.5. The average error bars in latitude, longitude and
304 depth are of the order of 3.40 km, 4.75 km and 4.5 km, respectively. The relocation of
305 large events (Mw >5.5) recorded by our OBS, which were also relocated by Engdahl et
306 al. (2007), shifted by ~10 km, ~25 km, ~2 km in longitude, latitude and depth,
307 respectively. Therefore, one should be cautious about using teleseismically located
308 events. However, dip of events are well constrained. Here, we combine all the
309 information to get insight about active deformation at depth.
310
311 About 400 accurately located micro-earthquakes are shown in Figure 1. There is a cluster
312 of micro-earthquakes at the front on profile WG2 and another cluster in the Aceh forearc
313 basin, south of profile WG2. On Figure 1, we also plot the CMT focal mechanism at the
314 epicentre of the teleseismic events between 1997 and 2005 relocated by Engdahl et al.
315 (2007). The depth distribution of the accurately relocated micro-earthquakes using OBS
316 data and teleseismic events are similar; therefore we believe that the depth of these
317 earthquakes is reasonable enough to interpret the two results jointly. As mentioned above,
318 there are steeply dipping thrust events near the subduction front. We projected the
319 teleseismic events and micro-earthquakes within 40 km of profile WG2 onto the depth

converted seismic profiles (Figure 7c). Seven teleseismic events project close to the reflector in the oceanic crust near the deformation front, consistent with the inference of active thrust faulting in the oceanic crust where it enters the subduction zone. The micro-earthquake cluster also lie at the same location. These micro-earthquakes coincide with the steeply dipping reflector imaged on the seismic profile. This faulting may be localised within the downgoing igneous oceanic crust near the front or may be due to the presence of megathrust within igneous oceanic crust (Singh et al., 2008).

Beneath the accretionary plateau, there are only a handful of micro-earthquakes within the accretionary wedge sediments, indicating that any deformation within the wedge is largely aseismic. There are several micro-earthquakes that align with reflector F1, suggesting that this interface might be active. The most of the micro-earthquakes in this area lie within the oceanic crust or below the oceanic Moho, indicating that the downgoing oceanic plate is actively deforming. There are a few micro-earthquake events that align with the backthrust, supporting the idea that the backthrust might have ruptured co-seismically during the 2004 great earthquake enhancing the tsunami (Chauhan et al., 2009; Singh et al. 2011b). We do not observe any micro-earthquake alignment dipping landward that could be interpreted as an out of sequence splay fault (Sibuet et al., 2007), consistent with the absence of any corresponding reflections on the seismic image.

Most of the teleseismic events and micro-earthquakes, however, occur below the Aceh forearc basin, either close to the plate interface (B2-F3) or within 20 km of it in the underlying oceanic lithosphere. There are many events aligned with reflector F3,

suggesting that there is some motion along this interface. Below F3, the focal mechanism dips of the teleseismic events are 25-30°, which is consistent with the dip of the best fitting line through the hypocentres in this region (~20°). Furthermore, the line connecting the flat reflector beneath the forearc high (F2) with the deepest flat reflector (F4) has a 20° dip and goes through these events, suggesting that an active thrust might be present, not necessarily at the top of the oceanic crust marked by F3. There are no earthquakes above reflector F4, and most of the earthquakes lie 10-15 km below it. The focal mechanisms of teleseismic events have a complex focal mechanism and possibly lie in the downgoing plate, similar to the 2009 Sumatra earthquake (McCloskey et al., 2010). There is a gap of 15 km laterally and 20 km vertically between the cluster of events below F3 and F4.

6. Discussion

Our results clearly show that the top of the downgoing plate is segmented containing bend (B) and flat reflectors (F) in at least three locations over a distance of 300 km as it descends from 15 km to 55 km (Figures7). The flat segment is ~50 km long, which cannot be an artefact of velocity uncertainties as our tomographic velocity is smooth. A dip of >20° (B1) is required to connect reflectors F1 and F2, ~15° (B2) for F2 and F3, and more than 30° (B3) for F3 and F4. The first bend occurs beneath the accretionary wedge where the plate deflects below a sliver of continental crust, which is stronger than the wedge sediments (Figure 8a). The second bend occurs where the subducting plate

365 encounters continental mantle beneath the edge of the Aceh forearc basin. The third, and
366 steepest, bend occurs in the mantle wedge near CDP 32500.
367
368 Although bending of the downgoing plate at its intersection with the continental crust and
369 Moho (e.g. B1 and B2) might be expected due to the change in lithology, unbending is
370 more difficult to explain, particularly at 55-60 km (F4) depth. However, flat subduction
371 has been observed in subduction zones such as South America (Barazangi and Isacks,
372 1997; Gustcher et al., 2000), Mexico (Saurez et al., 1990), southern Alaska (Brocher et
373 al, 1994). In these examples, the depth of initiation of flat subduction varies from 30 km
374 to 80 km, and the oceanic plate is flat over 100-300 km. On profile WG2 flat reflectors
375 are at shallower depths (15-60 km) and 50-60 km long. Several causes have been
376 proposed for flat subduction (Gutscher et al., 2000): for example, young subducting
377 lithosphere will be warm, and hence buoyant, and might result in flat subduction (Vlaar,
378 1983). However, beneath Sumatra the oceanic lithosphere is >60 Ma old. Anomalously
379 thick oceanic crust might also result in crustal buoyancy and flattening of the subducting
380 plate, but there is no evidence of thickened oceanic crust entering the subduction zone in
381 this region (Singh et al, 2011a). Crustal thickening might occur after the plate has entered
382 the subduction zone, but the thickness of the descending oceanic crust is not well
383 constrained at these depths by the refraction survey.
384
385 The flattening and bending of the top of the oceanic plate could also be produced by the
386 presence of large-scale subducted bathymetric features. Singh et al. (2011c) have imaged
387 a 4 km high 40 km wide subducted seamount at 30-40 km depth beneath the forearc

388 mantle. The frontal side of the seamount has a steep dip (20-30°) whereas the backside of
389 the seamount is nearly flat (Figure 8b). This is due to the dip of the plate interface and the
390 increase of velocity with depth. A seamount or bathymetric feature could be a maximum
391 of 4-5 km high and 50-60 km wide, and hence would produce a 20-30 km long
392 symmetric flat zone, but we observe 50-60 km long flat zones and 15-20 km steep zones
393 instead.
394
395 It is now well accepted that the subducting Indo-Australian plate in this region is actively
396 deforming, and the deformation is taking place along re-activated N-S fracture zones as
397 left lateral strike-slip motion (Deplus et al., 1998; Abercrombie et al. 2003). Graindorge
398 et al. (2008) suggest that such deformations of the downgoing oceanic plate continue
399 beneath the accretionary wedge, and therefore, one can argue that the steps we observe
400 along profile WG2 could be linked to the deformation along these fracture zones. The
401 maximum vertical offset observed along these re-activated fracture zones on the oceanic
402 plate is ~300 m (Singh et al., 2011a) whereas the steps we observe on profile WG2 are 5-
403 25 km. Although some N-S linear features are observed on the bathymetry (Graindorge et
404 al., 2008), they are very small for steps of 5-15 km, and therefore it is very unlikely that
405 these steps are related to re-activation of the fracture zones.
406
407 The change in the dip at the top of the subducting plate is likely to affect the inter-plate
408 coupling, and hence the width of the seismogenic zone. It has been observed that the
409 seismicity above the flat part of a subduction zone is 3-5 times greater than the adjacent
410 steep part (Jordan et al., 1983; Gutscher et al., 2000), and the focal mechanisms of these

411 events are predominantly compressional (thrust) to transcurrent (strike-slip) suggesting
412 that the subduction plate boundary stresses are transmitted to the upper plate. Since the
413 surface area of the flat part of the interface is larger than the steep part, the plate
414 boundary forces are transmitted more effectively to the upper plate. In our case, the flat
415 reflector F1 and F3 have earthquakes but F2 and F4 do not seem to have any earthquake
416 above them. The deepest part of the 2004 earthquake rupture was deeper than reflector
417 F2, and hence this hypothesis may not be valid here.
418
419 The flattened reflectors could also be produced by faulting of the oceanic crust as it
420 subducts. The staircase reflectors could be easily produced by normal faulting (Figure
421 8c), but we do not observe any normal earthquake in the region. Singh et al. (2008) have
422 shown the seismic image of thrust faulting in the oceanic crust further south near the
423 2004 earthquake epicentre. The presence of steeply dipping thrust earthquakes near the
424 deformation front, collocated with a landward dipping seismic reflector in the oceanic
425 crust on profile WG2, supports the idea of thrust faulting (Figure 8d). Similarly, most of
426 the events beneath the Aceh basin have steeply dipping thrust focal mechanism, further
427 supporting the idea of thrusting within the oceanic crust and upper mantle. Recently,
428 Singh et al. (2011d) have shown thrusting of oceanic crust near the subduction front in
429 Southern Sumatra.
430
431 In any case, the change in the dip at the top of the oceanic crust is likely to create a thrust
432 cutting through the oceanic crust and mantle (Figure 8e), leading to a mantle megathrust
433 as suggested by Singh et al. (2008). Once the megathrust extends into the oceanic plate,

434 oceanic crustal and mantle material can be underplated to the overriding plate as the
435 megathrust evolves (Calvert, 2004; Calvert et al., 2006), and the geometry of the top of
436 the igneous crust under the accretionary wedge may become complex. The presence of
437 steeply dipping aftershocks beneath the top of the oceanic crust between CDP 27000 and
438 32000 suggests that the present megathrust might be in the mantle and this part of the
439 oceanic crust might be underplated material. Just south of this survey, Singh et al. (2008)
440 observed a pair of reflectors above the oceanic plate, which they interpreted to be
441 underplated oceanic crust. We speculate that the exhumed ophiolites identified on the
442 Mentawai-Andaman island chain may be the long-term outcome of successive episodes
443 of underplating (Singh et al., 2008; 2010). The underplating has also been reported along
444 the central Japan subduction zone (Kumara et al., 2010).
445
446 The underplating hypothesis is further indicated by the high free air gravity anomaly at
447 the southwestern half of the accretionary wedge and the seismic reflection image.
448 Although the average water depth of the 125 km wide plateau is ~1400 m, the free air
449 gravity anomaly has two distinct features; a positive gravity anomaly of 50 mgal from
450 100 to 150 km distance, and a negative anomaly of –50 mgal from 175 to 230 km
451 distance (Figure 9), which also coincides with reflectors F1 and F2 and bathymetric
452 slopes S1 and S2. The negative gravity anomaly is explained by the presence of thick
453 sediments whereas the positive anomaly requires high-density material at depth, such as
454 the underplating of oceanic crust and mantle (Figure 9). The slope in gravity anomaly lies
455 exactly at bend B1, which has a step of 8 km. We have modelled these gravity data,
456 which is consistent with the possible presence of serpentinized peridotite along the profile

457 and support the underplating of the oceanic crust and upper mantle being the cause of the
458 uplift of the accretionary plateau. The presence of undisturbed 3 km thick accreted
459 sediments NE of the frontal ridge (Figure 3a) suggest that these sediments have been
460 uplifted intact supporting the idea of underplating and megathrust in the mantle (Figure
461 10) along the seismic reflection image at 20 km depth.
462
463 The present position of the megathrust beneath the Aceh basin is not very clear. Although
464 there are some seismic events at the top of the oceanic crust, most of them lie below this
465 reflector. The dip of the earthquakes, the line joining these events, and line connecting F2
466 and F4 all have a dip of 20-30°, suggesting that the megathrust should lie along this line.
467 Gravity data is consistent with the possible presence of serpentinized peridotite above this
468 line (Figure 8). To explain complex reflectors at similar depths in the Cascadia
469 subduction zone, Calvert et al. (2004, 2006) has proposed the existence of a mega-duplex
470 structure in a complex inter-plate boundary zone, which can result in a transfer of oceanic
471 crust from the descending plate to the overriding forearc crust. The observed reflectors
472 and the pattern of aftershock seismicity are consistent with a similar feature at depths of
473 30-45 km beneath the Aceh forearc basin. Monie and Agard (2009) have reported the
474 presence of the oceanic blueschist along the Neotethyan subduction zone, from Zagros to
475 the Himalayas over 3000 km distance range that seem to have been exhumed from 30-40
476 km depths long before the collision, suggesting breaking of the oceanic crust and
477 underplating.
478

Since the top of the oceanic crust is imaged down to 60 km depth along profile WG2, this must have been transported (subducted) to these depths, which means that the mantle megathrust and underplating process proposed here have to be short lived. The presence of subducted bathymetric features (Singh et al., 2011c) or thrusts within the oceanic plate (Singh et al., 2008) may produce a difference in coupling along the plate interface causing the slicing of the oceanic topographic features during great megathrust earthquakes (Mw>9) leading to the development of mantle megathrust and subsequent underplating (Figure 10). Once megathrust is well established, this becomes the main plate boundary interface where great earthquakes can originate, whereas small earthquakes may still occur on the top of the oceanic crust. However, we cannot rule out of the possibility of the meagthrust being at top of oceanic crust (Figure 10), but it is certain that the downgoing oceanic crust and upper mantle deform actively, which would require some other explanations.

The complex geometry of the top of the oceanic crust and the seismogenic zone would also affect the size of earthquakes and fault segmentation. In Southern Sumatra, a twin earthquake occurred in a 12-hour interval on September 12, 2007. The first one, Mw=8.4, broke the upper part of the plate boundary at 10-20 km depth km whereas the second one, Mw=7.9, broke the lower part of the plate boundary at 20-40 km (Singh et al., 2010; Konka et al., 2008). Recently, a third earthquake occurred in 2010, which broke the frontal section of the subduction zone that requires the megathrust to be in the oceanic lithosphere (Singh et al., 2011d). The bending and unbending of the downgoing plate would facilitate the segmentation of earthquakes in the dip direction and the initiation of

502 the megathrust in the oceanic mantle, which may lead to the exceptional size of the
503 earthquake as suggested by Singh et al (2008). The presence of mantle megathrust would
504 increase the upper limit of the seismogenic zone towards the subduction front. The shape
505 of the downgoing plate would also affect modelling of the co-seismic and interseismic
506 slip in the region (Chlieh et al., 2007; Chlieh et al., 2008) as well as the thermal
507 modelling studies (Hippchen and Hyndman, 2008). It would also affect the melting zone
508 beneath the volcanic arc. For example, Chlieh et al. (2007) suggest that the top of the
509 oceanic plate beneath the volcanic arc should be at >110 km depth whereas our results
510 require it to be 70-80 km depth.
511
512 **7. Conclusions**
513
514 We have shown the very first detailed seismic image of the Sumatran subduction system
515 from the subduction front to the volcanic arc from the seafloor down to 60 km depth. Our
516 results show that the top of the subducting oceanic plate is segmented in a form of
517 staircase containing ~50 km long shallow dipping segments at 5-15 km depth interval.
518 The presence of a large number of aftershock hypocentres below this interface indicates
519 that the downgoing oceanic plate is deforming. We have also imaged a thrust near the
520 subduction front in the oceanic plate that might have ruptured during the 2004 earthquake
521 uplifting the water column at 4.5 km water depth producing the devastating tsunami in
522 the Indian Ocean region. We have also imaged a reflection in the oceanic mantle, which
523 might be the mantle megathrust suggested by Singh et al. (2008). The high accretionary
524 plateau might be due to uplifting of the oceanic material along this megathrust.

Aftershocks data suggest that the megathrust beneath the forearc mantle is not at the top of the oceanic crust but cuts through the oceanic mantle and crust. We suggest the mantle megathrusts develop during great megathrust earthquakes that are capable of slicing through topographic features on the downgoing plate and is short lived.

Acknowledgements

The seismic reflection data acquisition and processing were funded by WesternGeco. The refraction survey was carried out on the French R/V *Marion Dufresne* and funded by the French Agence Nationale de Recherche. Funding to AC was partly provided by the Natural Sciences and Engineering Council of Canada. Institut de Physique du Globe de Paris contribution number x.

References

Abercrombie, R.E., Antolik, M., Ekstrom, G., 2003. The June 2000 Mw 7.9 earthquakes south of Sumatra: deformation in the India-Australia Plate. J. geophys. Res. 108, 2018, doi:10.1029/2001JB000674.

Ammon, C.J., et al., 2005. Rupture process of the 2004 Sumatra-Andaman earthquake. Science 308, 1133-1139.

Avedik, F., Renard, V., Allenou, J., Morvan, B., 1993. Single bubble air-gun array for deep exploration. Geophysics 58, 366-382.

Araki, E., Shinohara, M., Obana, K., Yamada, T., Kaneda, Y., Kanazawa, T., Suyehiro,

548 K., 2006. Aftershock distribution of the 26 December 2004 Sumatra-Andaman
549 earthquake from ocean bottom seismographic observation. Earth Planets Space 58,
550 113–119.
551 Barazangi, M., Isacks, B., 1976. Spatial distribution of earthquakes and subduction zone
552 and subduction of the Nazca Plate beneath South America. Geology 4, 686-692.
553 Brocher, T., Fuis, T.S., Fisher, M.A., Plafker, G, Moses, M.J., 1994. Mapping the
554 megathrust beneath the northern Gulf of Alaska using wide-angle seismic data. J.
555 Geophys. Res. 99, 11663-11685.
556 Calvert, A.J., Ramachandran, K., Kao, H., Fisher, M.A., 2006. Local thickening of the
557 Cascadia forearc crust and the origin of seismic reflectors in the uppermost mantle.
558 Tectonophysics 420, 175-188.
559 Calvert, A.J., 2004. Seismic reflection imaging of two megathrust shear zones in the
560 northern Cascadia subduction zone. Nature, 428, 164-167.
561 Chauhan, A. S., Singh, S.C., Hananto, N., Carton, H., Klingelhoefer, F., Dessa, J,-X.,
562 Permana, H., White, N.J., Graindorge, D. & Sumatra OBS Scientific Team, 2009.
563 Seismic imaging of forearc backthrusts at northern Sumatra subduction zone.
564 Geophys. J. Int. 179, 1772-1780.
565 Chlieh, M. et al., 2007. Coseismic and afterslip of the great Mw 9.15 Sumatra-Andaman
566 earthquake of 2004. Bull. Seism. Soc. Am. 97, S152-S173.
567 Dean, S. M, McNeill, L.S., Henstock, T.J., Bull, J.M., Gulick, S., Austin, J., Bangs, N.,
568 Djajadihardja, Y., Permana, H., 2010. Contrasting decollement and prism properties
569 over the Sumatra 2004-2005 earthquake rupture boundary. Science 329, 207-210.

570 Deplus, C., *et al*., 1998. Direct evidence of active deformation in the eastern Indian
571 oceanic plate. Geology 26, 131-134.
572 Dessa, J.X., Klingelhoefer, F., Graindorge, D., Andre, C., Permana, H., Gutscher, M.A.,
573 Chauhan, A., Singh, S.C. and the SUMATRA-OBS Scientific Team, 2009.
574 Megathrust earthquakes can nucleate in the forearc mantle: Evidence from the 2004
575 Sumatra event. Geology 37, 659-662.
576 Dewey, J.W. et al., 2007. Seismicity associated with the Sumatra-Andaman Islands
577 earthquake of 26 December 2004. Bull. Seism. Soc. Am. 97, S25-S42.
578 Diament, M., Harjono, H., Karta, K., Deplus, C., Dahrin, D., Zen, M. T., Gerard, M.,
579 Lassal, O., Martin A., Malod, J., 1992. Mentawai fault zone off Sumatra - a new
580 key to the geodynamics of western Indonesia. Geology 20, 259-262.
581 Engdahl, E.R., Villasenor, A., DeShon, H.R., Thurber, C.H., 2007. Teleseismic relocation
582 and assessment of seismicity (1918-2005) in the region of the 2004 Mw 9.0
583 Sumatra-Andaman and the 2005 Mw 8.6 Nias Island Great earthquakes. Bull.
584 Seism. Soc. Am. 97, S1-S19.
585 Fitch, T., 1972. Plate Convergence, Transcurrent Faults, and Internal Deformation
586 Adjacent to Southeast Asia and the Western Pacific. J. Geophys. Res. 77, 4432–
587 4462.
588 Franke, D. *et al*., 2008. The great Sumatra-Andaman earthquakes-Imaging the boundary
589 between the ruptures of the great 2004 and 2005 earthquakes. Earth Planet. Sci.
590 Lett. 269, 119-130.
591 Foster, D. J., Mosher, C. C., 1992. Suppression of multiple reflections using the Radon transform.
592 Geophysics 57, 386-395.

593 Ghosal, D., Singh, S.C., Chauhan, A.P.S., Hananto, N. D., 2009. New insight on the
594 Great Sumatra Fault, offshore NW Sumatra, from recent marine data. Eos Trans.
595 AGU, 90(52), Fall Meet. Suppl., Abstract T33B-1917.
596 Graindorge, D., et al., 2008. Impact of lower plate structure on upper plate deformation
597 at the NW Sumatran convergent margin from seafloor morphology. Earth Planet.
598 Sci. Lett. 275, 201-210.
599 Gutscher, M-A, Spakman, W., Bijwaard, H., Engdahl, E.R., 2000. Geodynamics of flat
600 subduction: Seismicity and tomographic constraints from the Andean margin.
601 Tectonics 19, 814-833.
602 Hamilton, W. B., 1988. Plate tectonics and island arcs, Bull. Geol. Soc. Am. 100, 1503-
603 1527.
604 Henstock, T.J., McNeill, L.C. Tappin, D.R., 2006. Seafloor morphology of the Sumatran
605 subduction zone: Surface rupture during megathrust earthquakes? Geology 34, 485–
606 488.
607 Hippchen, S., Hyndman, R.D, 2008. Thermal and structural models of the Sumatra
608 subduction zone: Implications for the megathrust seismic zone. J. Geophys. Res.
609 113, B12103, doi:10.1029/ 2008JB005698.
610 Hobro, J, Singh, S. C., Minshull, T. A., 2003. Three-dimensional tomographic inversion
611 of combined reflection and refraction seismic traveltime data, Geophys. J. Int. 152,
612 79-93.
613 Hyndman, R.D., Wang, K, Yamano, M., 1995. Thermal constraints on the seismogenic
614 portion of the southwestern Japan subduction thrust. J. Geophys. Res. 100, 15373-
615 15392.

616 Jordan, T., Isacks, B., Allmendinger, Brewer, J.A., Ramos, V.A., Ando, C.J., 1983.
617 Andean Tectonics related to geometry of subducted Nazca plate. Geol. Soc. Am.
618 Bull. 94, 341-361.
619 Kamesh Raju, K. A., Ramprasad, T., Rao, P. S., Rao, B. R., Varghese, J., 2—4. New
620 insights into the tectonics evolution of the Andaman basin, northeast Indian Ocean,
621 Earth Planet. Sci Lett. 7024, 1-18.
622 Katili, J., 1973. Geochronology of West Indonesia and its implication on plate tectonics,
623 Tectonophysics 19, 195-212.
624 Konca, A.O. et al., 2008. Partial rupture of a locked patch of the Sumatra megathrust
625 during the 2007 earthquake sequence. Nature 456, 631-635.
626 Kimura, H., Takeda, T., Obara, K., Kasahara, K., 2010. Seismic evidence for active
627 underplating below the megathrust earthquake zone in Japan, Science 329, 210-211.
628 Lienert, B. R. E., Berg, E., Frazer, L. N., 1986. Hypocenter: An earthquake location
629 method using centered, scaled, and adaptively least squares. B. Seismol. Soc. Am.
630 76, 771–783.
631 McCloskey J., Lange, D., Tilmann, F., Nalbant, S., Bell, A., Natawidjaja, D., Rietbrock,
632 A., 2010. The September 2009 Padang earthquake. Nature Geoscience 3, 70-71.
633 McCaffrey, R., Zwick, P. C., Bock, Y., Prawirodirdjo, L., Genrich, J. F., Stevens, C. W.,
634 Puntodewo, S. S., Subarya, C., 2000. Strain partitioning during oblique plate
635 convergence in northern Sumatra: Geodetic and seismologic constraints and
636 numerical modeling, J. Geophys. Res. 105, 28363-28376.
637 Pesicek, J. D., Thurber, C. H., Zhang, H., DeSon, H. R., Engdahl, E. R., Widiyantoro, S.,
638 2010. Teleseismic double-difference relocation of earthquakes along the Sumatra-
639 Andaman zone. J. Geophys. Res. 115, B10303, doi:10.1029/2010JB007443.

640 Rhie, J., Dreger, D, Bürgmann, R., & Romanowicz, B., 2007. Slip of the 2004 Sumatra-
641 Andaman earthquake from joint inversion of long-period global seismic waveforms
642 and GPS static offsets. Bull. Seis. Soc. Am. 97, S115-S127.
643 Sacks, I.S., 1983. The subduction of young lithosphere. J. Geophys. Res. 88, 3355-3366.
644 Sibuet, J.-C. et al., 2007. 26th December 2004 Great Sumatra-Andaman Earthquake:
645 seismogenic zone and active splay faults. Earth Planet. Sci. Lett. 263, 88-103.
646 Sieh, K., and. Natawidjaja, D., 2000. Neotectonics of the Sumatran fault, Indonesia. J.
647 Geophys. Res. 105, 28,295-228,326.
648 Singh, S.C., et al., 2005. Sumatra earthquake research indicates why rupture propagated
649 northward. Eos 86, 497-502.
650 Singh, S. C., Carton, H., Tapponier, P., Hananto, N., Chauhan, A.P.S., Hartoyo, D.,
651 Bayly, M., Moeljopranoto, S., Bunting, T., Christie, P., Lubis, H., Martin, J. 2008.
652 Seismic evidence for broken oceanic crust in the 2004 Sumatra earthquake
653 epicentral region. Nature Geoscience 1, 771-781.
654 Singh, S. C., Hananto, N., Chauhan, A.P.S., Permana, H. Denolle, M., Hendriyana, A.,
655 Natawidjaja, D., 2010. Evidence of active backthrusting at the NE Margin of
656 Mentawai Islands, SW Sumatra. Geophys. J. Int. 180, 703-714.
657 Singh, S.C. et al., 2011a. Extremely thin crust in the Indian Ocean possibly resulting from
658 Plume-Ridge interaction. Geophys. J. Int. 184, 29-42.
659 Singh, S.C., Hananto, N., Chauhan, A., 2011b. Enhanced reflectivity of backthrusts in the
660 recent great Sumatran earthquake rupture zones. G.R.L. 38*, L04302,*
661 doi:10.1029/2010GL046227.
662 Singh, S.C. et al., 2011c. Aseismic zone and earthquake segmentation associated with a
663 deep subducted seamount in Sumatra. Nature Geoscience 4*,* doi:10.1038/NG01119.

664 Singh, S.C., Hanato, N., Mukti, M, Permana, H., Djajadihardja, Y., Harjono, H., 2011d.
665 Seismic images of the megathrust rupture during the 25th October 2010 Pagai
666 earthquake, SW Sumatra: Frontal rupture and large tsunami. G.R.L. 38, L16313,
667 doi:10.1029/2011GL048935.
668 Suarez, G., Montfret, T., Wittlinger, G. David, C., 1990. Geometry of subduction and
669 depth of the seismogenic zone in the Guerrero gap, Mexico. Nature 345, 336-338.
670 Thurber, C., Eberhart-Phillips, D., 1999. Local earthquake tomography with flexible
671 gridding. Comput. Geosci. 25, 809-818.
672 Thurber, C. H., 1992. Hypocenter-velocity structure coupling in local earthquake
673 tomography. Phys. Earth Planet. Int. 75, 55-62.
674 Trinks, I., Singh, S.C., Chapman, C., Barton, P.J., Bosch, M., 2005. Adaptive travel time
675 tomography of densely sampled seismic data. Geophys. J. Int. 160, 925-938.
676 Vlaar, N.J., 1983. Thermal anomalies and magmatism due to lithospheric doubling and
677 shifting. Earth Planet. Sci. Lett. 65, 322-330.
678
679
680
681 **Figure Captions**
682
683 Figure 1: Study Area: Bathymetry compiled from Henstock et al. (2006) and Graindorge
684 et al. (2008) superimposed onto GEBCO grid in the background. Black line is
685 WesternGeco seismic reflection profile WG2, red dots indicate OBS locations for seismic
686 refraction survey and brown dots OBS locations for aftershocks study (Sibuet et al.,

687 2007). Red dotted contours represent the10 m slip contour from Chlieh et al. (2007) and
688 black dotted contours the 30 m slip contour from Rhie et al. (2007), associated with the
689 2004 earthquake. Black dots are our aftershock locations and beach balls are CMT
690 solution corresponding to earthquake locations from Engdahl et al (2007). Blue: Thrust,
691 Green: Strike-slip and Red: Normal faulting mechanism. Location of the 2004 great
692 earthquake epicentre is marked by black beach ball. WAF: West Andaman Fault.
693
694 Figure 2: Deep seismic image: (a) Bathymetric profile along profile WG2. Light red
695 colour lines are slope on accretionary plateau (S1, S2). (b) Non-interpreted deep seismic
696 reflection image along profile WG2, and (c) interpreted seismic profile. Green lines:
697 sedimentary structure, Red: Igneous crust, Moho and mantle reflectors, Black: Crustal
698 faults and reflectors. The blue box indicates the location of seismic images shown in
699 Figure 3.
700
701 Figure 3: Blow up of seismic image: (a) Frontal section and (b) forearc high and Aceh
702 Basin. Green: sediments; Red: Crustal and mantle reflectors; Black: faults and dipping
703 reflectors.
704
705 Figure 4: (a) Bathymetry along the OBS profile. Red circles denote the position of OBS
706 used during the survey, and green circle the position of OBS data shown in Figure 5. (b)
707 An example of OBS data. Brown dashed curves highlight the main arrivals. Paccr: P-
708 wave arrival turning in accretionary sediments, Ptop: Reflection arrival from the top of

709 the oceanic crust, Pbs: Reflection from the back thrust, Pg: Crustal arrival, Pn: mantle
710 arrival.
711
712 Figure 5: (a) Observed travel time (red) and computed travel time (green) after the
713 inversion. (b) Travel time residuals: Red: Initial, Green: After three iterations and Blue:
714 Final residual.
715
716 Figure 6: (a) Final inverted velocity model, (b) Ray density plot and (c) uncertainty in
717 velocity estimation. The numbers along the contour indicate velocity (a) and uncertainty
718 (c). Purple line indicates results from wide-angle reflection data.
719
720 Figure 7: (a) Non-interpreted depth converted seismic reflection image and velocity
721 model determined using tomography (colour). Velocity contours are marked with white
722 line, numbers indicating velocities. Purple line indicates results from wide-angle
723 reflection. (b) Interpreted depth converted seismic image. Black lines mark the coherent
724 reflectors in the upper plate and faults, red lines: igneous crust, Moho and mantle
725 reflections; Purple line: Results from wide-angle reflection; Thin black line: velocity
726 contours shown in Figure a. (c) Projected earthquakes and aftershocks on profile WG2.
727 Grey dots are our micro-earthquake locations and black dots are earthquakes from
728 Engdahl et al (2007). Beach balls are CMT fault plane solutions: Red: Thrust, Blue:
729 Strike-slip and Green: Normal. Thick Red: Interpreted top of oceanic crust; Dashed Red;
730 Interpreted Continental Moho; Thick dashed grey line: position of the mantle megathrust;
731 Thin dashed grey line: Backthrust; Thin grey line: Sumatra fault at depth.

732

733 Figure 8: Different possible models for flattened and bend oceanic crust. Bending due to
734 (a) rheology, (b) seamount, (c) normal faulting, (d) thrust faulting, (e) and generation of
735 mantle megathrust.

736

737 Figure 9: (a) Gravity data and modelled response along profile WG2 along with
738 bathymetry (blue), (b) density model of the earth.

739

740 Figure 10: Schematic diagram of the structural units along profile WG2 showing staircase
741 pattern of the subducting oceanic crust. Thick dashed black line indicates the possible
742 position of mantle megathrust and thin dashed black line: Backthrust. Beach balls the
743 hypocentres shown in Figure 7c.

744

745

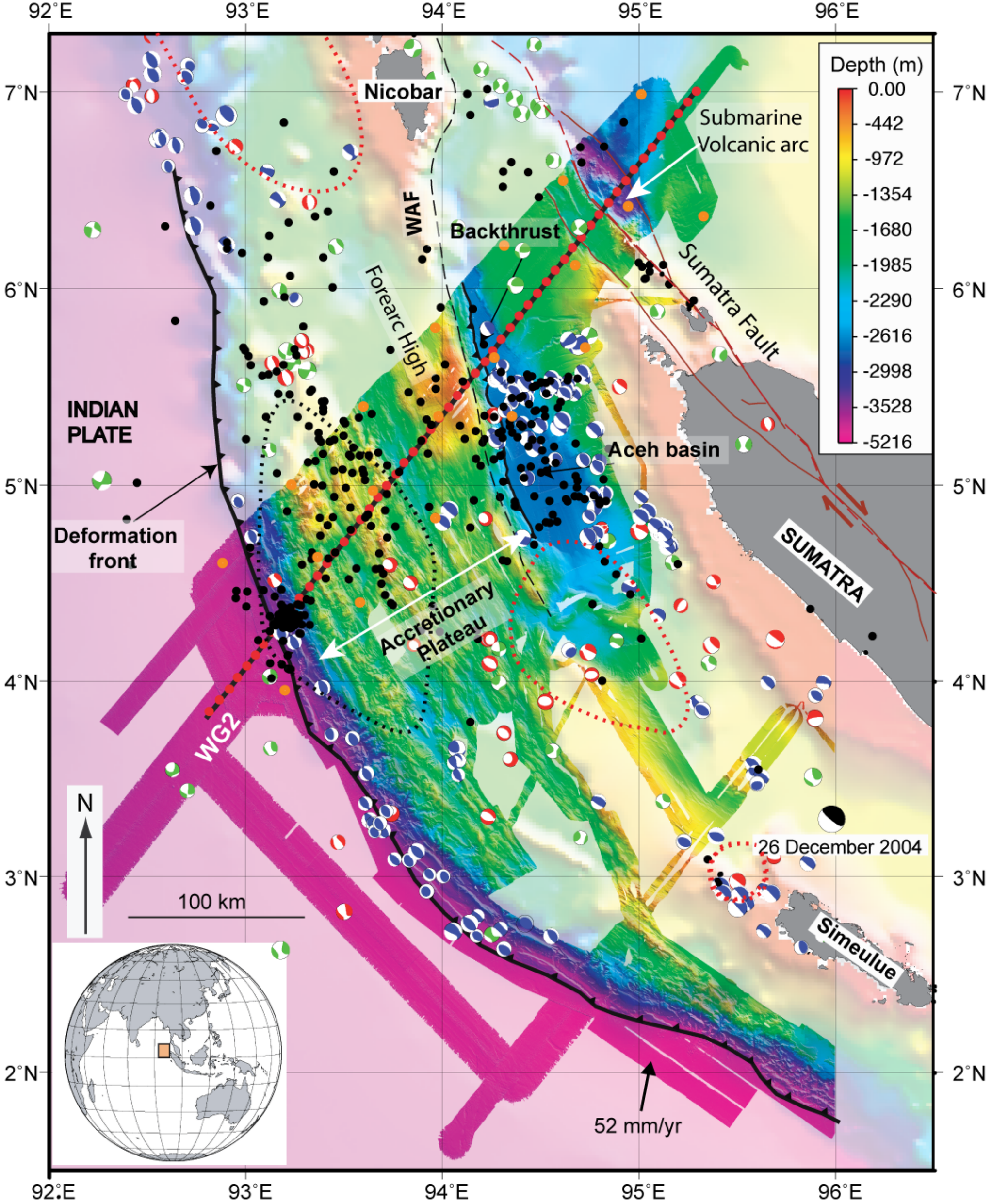

Singh et al., Figure 1

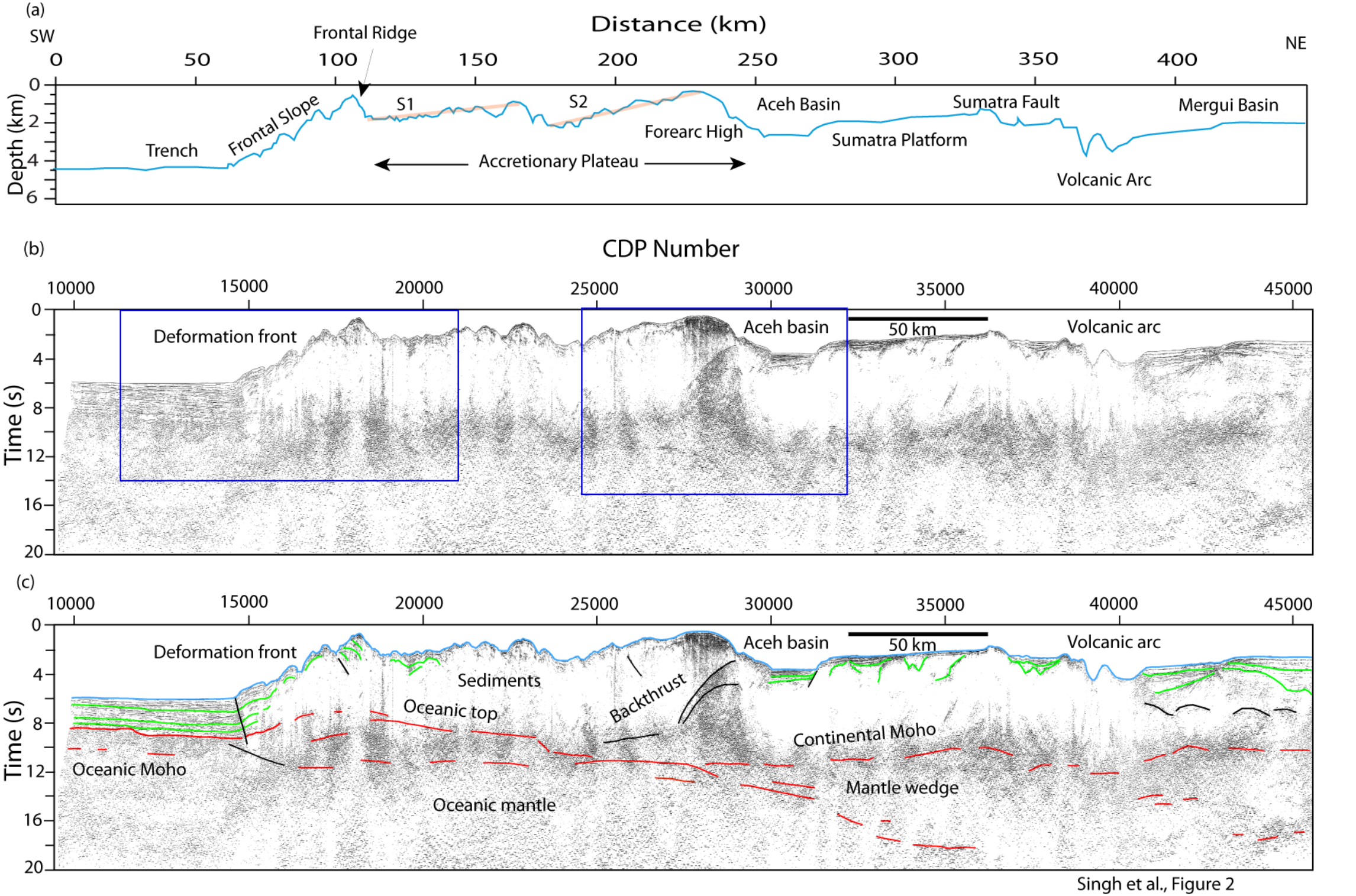

Singh et al., Figure 2

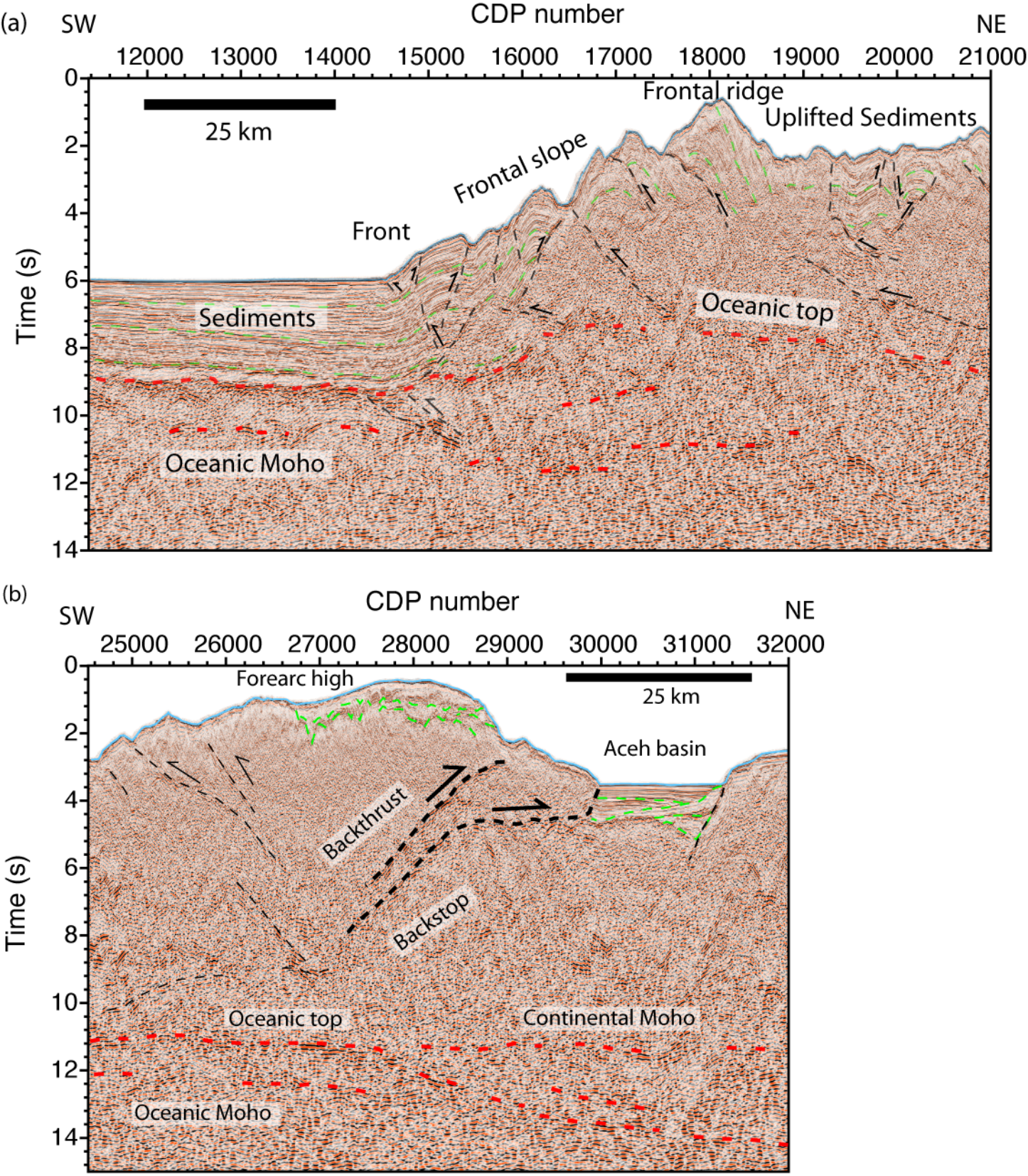

Singh et al., Figure 3

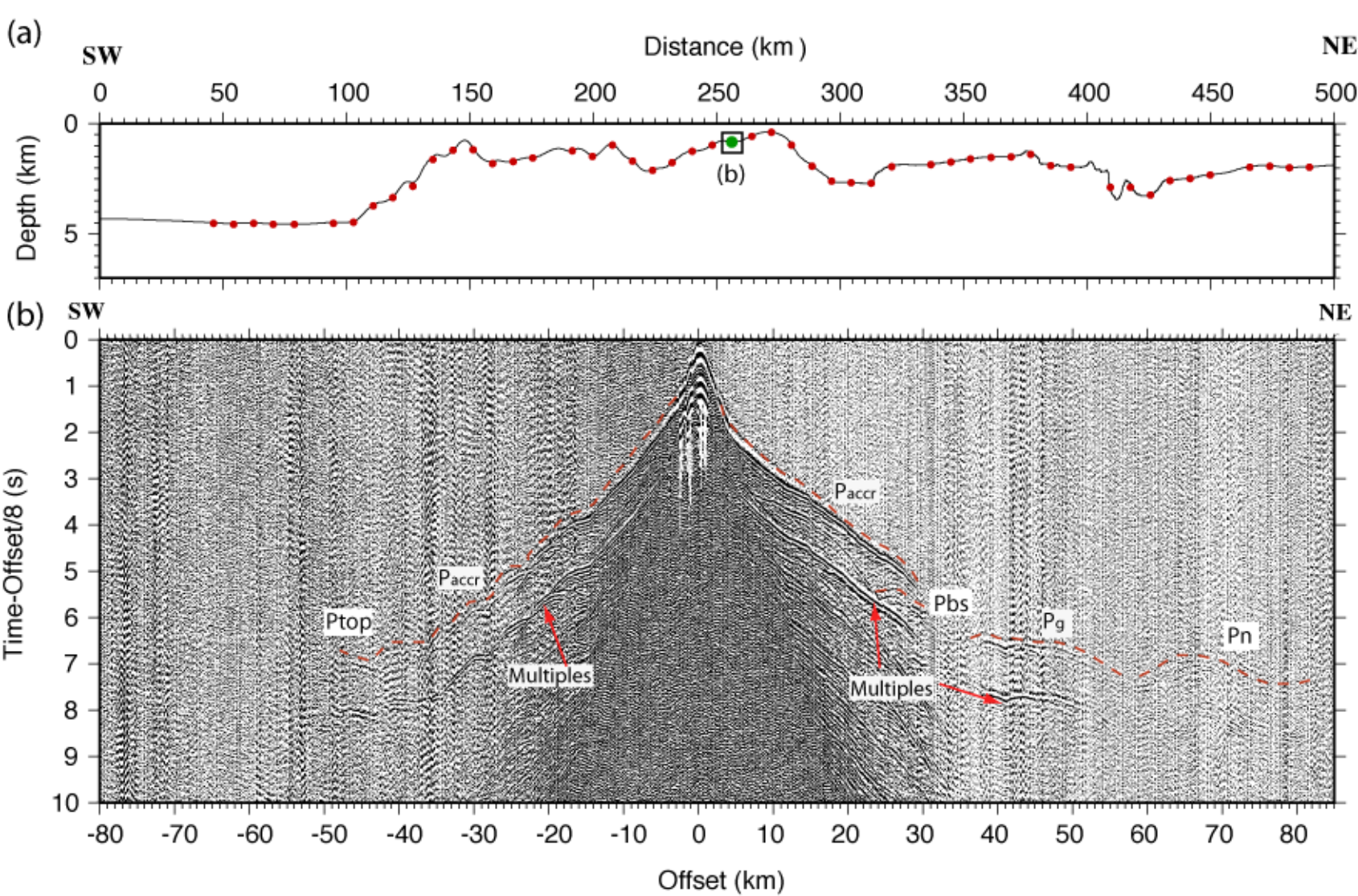

Singh et al. Figure 4

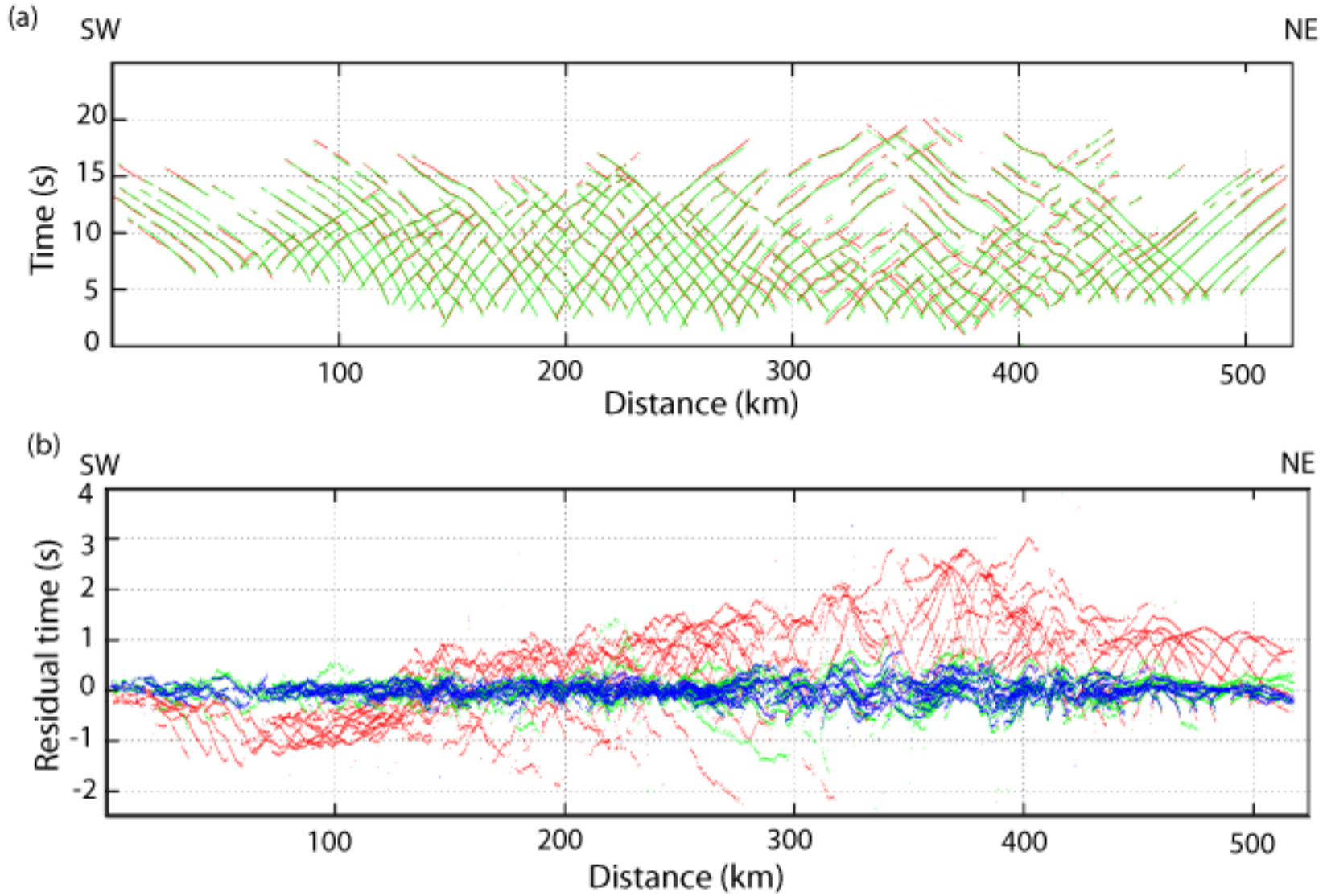

Singh et al. Figure 5

Singh Figure 6

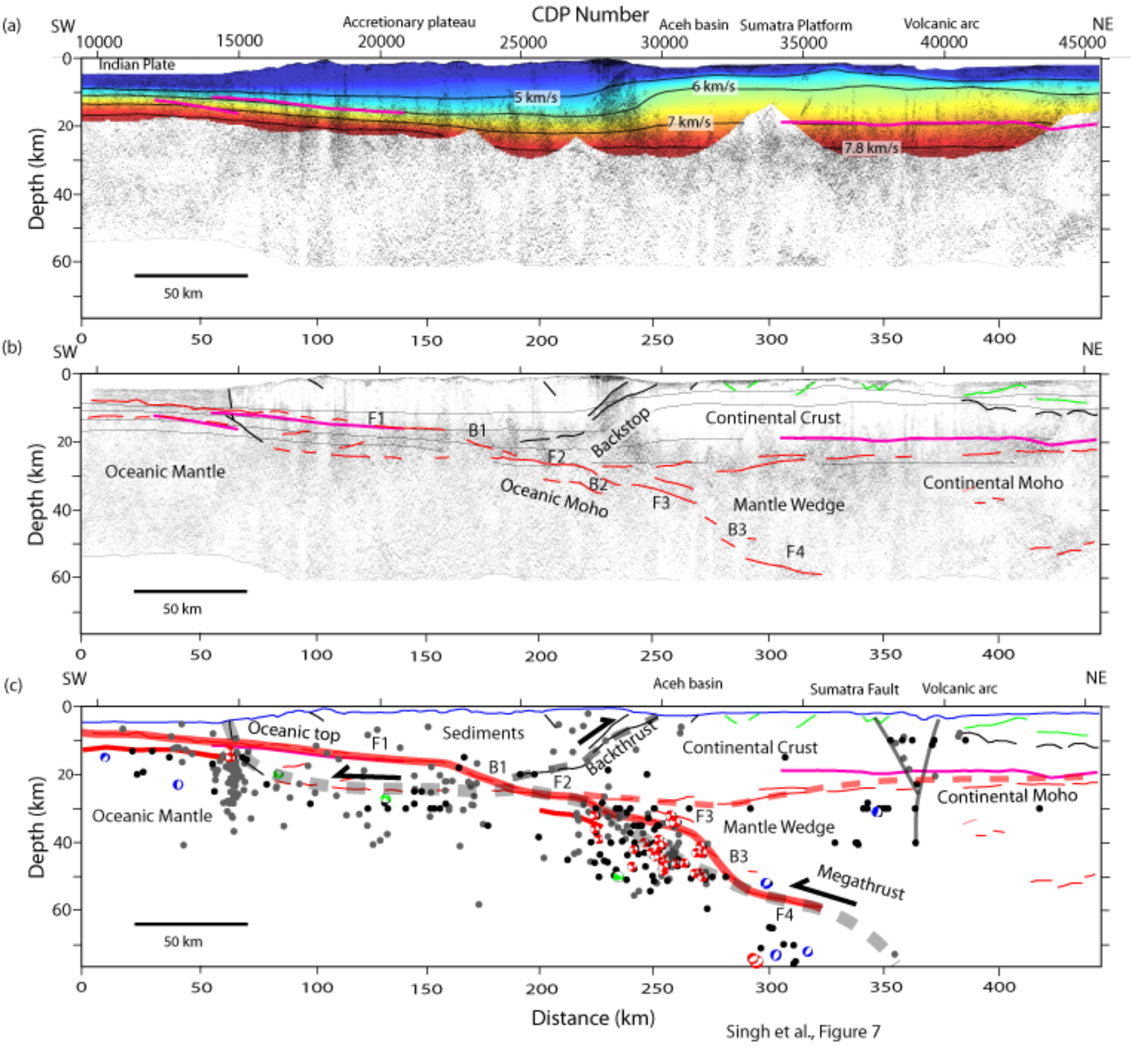

Singh et al., Figure 7

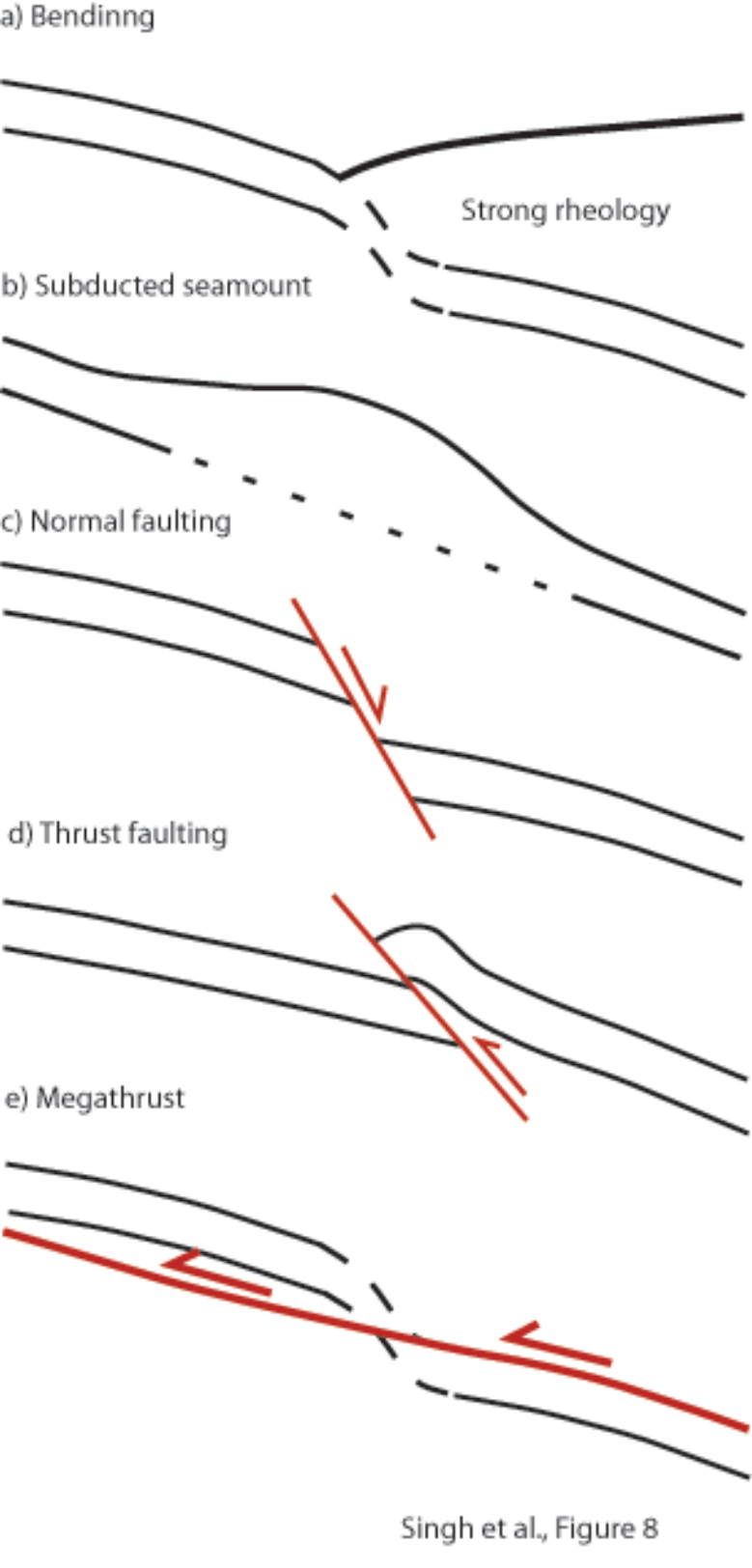

Singh et al., Figure 8

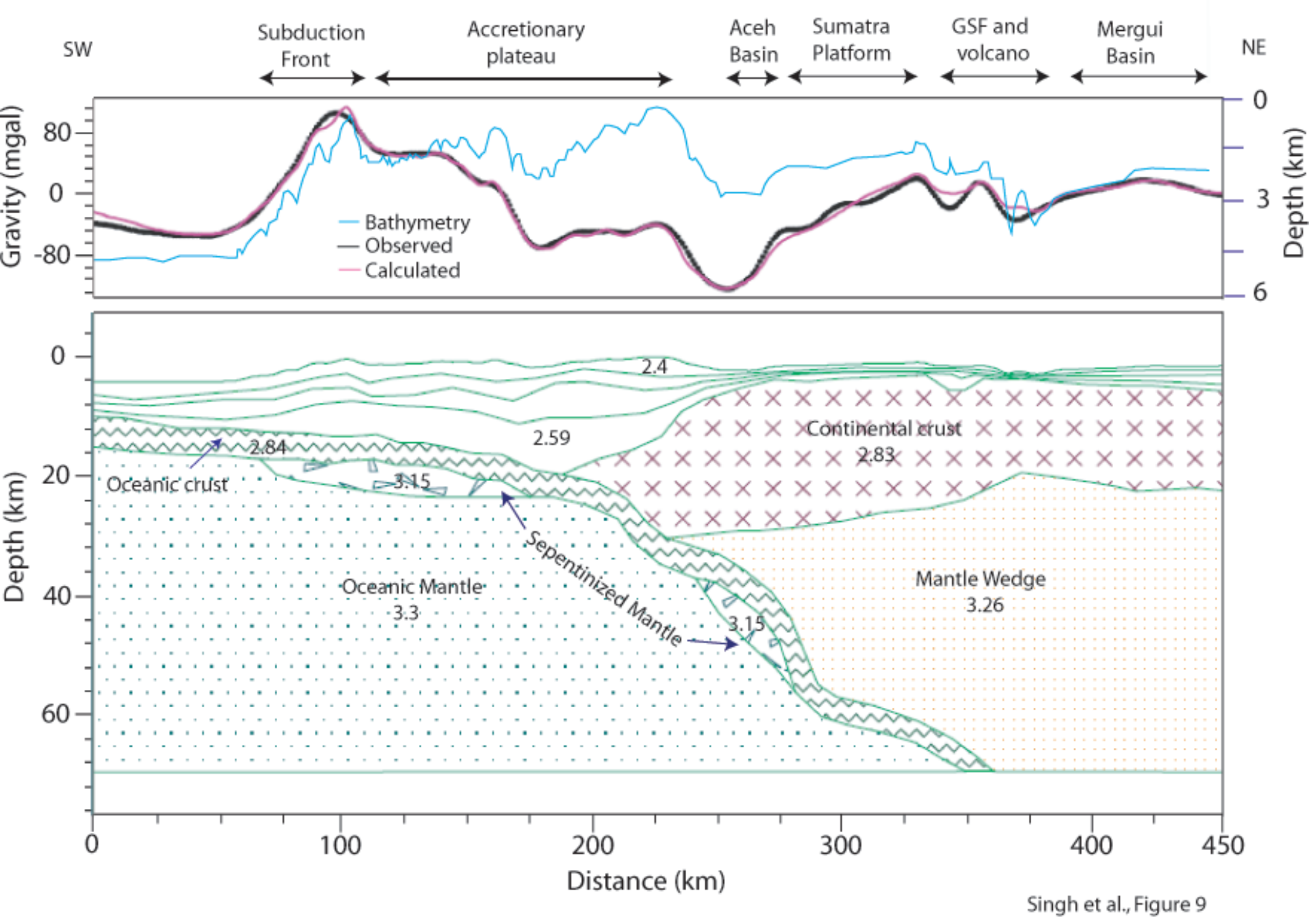

Singh et al., Figure 9

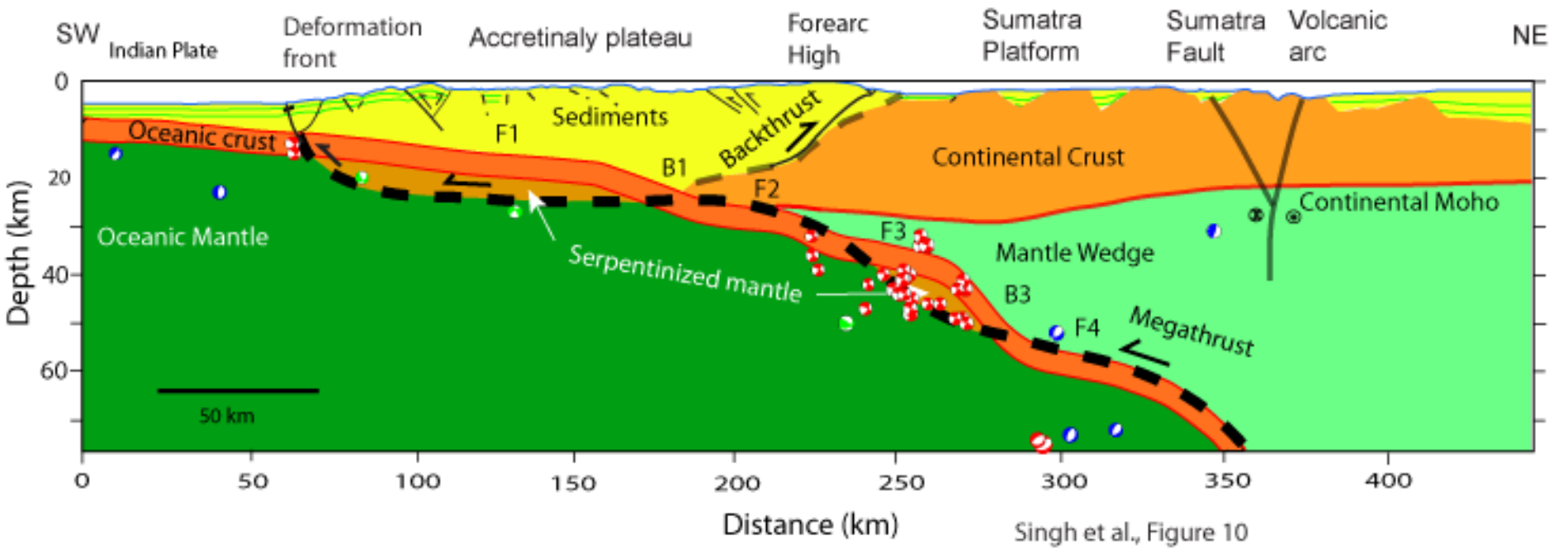

Singh et al., Figure 10